Available online at www.sciencedirect.com
ScienceDirect
Journal of Catalysis 256 (2008) 159–171
JOURNAL OF CATALYSIS
www.elsevier.com/locate/jcat

Activation and isomerization of hydrocarbons over WO_3/ZrO_2 catalysts II. Influence of tungsten loading on catalytic activity: Mechanistic studies and correlation with surface reducibility and tungsten surface species

François Di Gregorio, Nicolas Keller, Valérie Keller *

LMSPC, Laboratoire des Matériaux, Surfaces et Procédés pour la Catalyse and ELCASS, European Laboratory for Catalysis and Surfaces Sciences, 25, rue Becquerel 67087, Strasbourg Cedex 2, France

Received 30 October 2007; revised 27 December 2007; accepted 27 February 2008

Abstract

We studied the correlation among the catalytic behavior of WO_3/ZrO_2 samples toward unsaturated and saturated hydrocarbons transformation, tungsten surface species oxidation states, and the crystallographic structure of the zirconia support. Different tungsten-loaded catalysts were studied, from 9 wt% (near-monolayer coverage) to 30 wt%. The resulting WO_3/ZrO_2 materials were obtained by impregnation of a tungsten salt on either a commercially available monoclinic zirconia or an amorphous hydroxide, $ZrO_x(OH)_{4-2x}$, followed by a calcination step (according to the Hino and Arata procedure), leading to a tetragonal structure. In contrast to previous works, here we demonstrate that the crystallographic structure of zirconia has no influence on catalytic properties. Correlations with XPS analyses revealed two aspects of catalytic behavior that depend strongly on the catalyst reducibility and thus on the W surface species oxidation states. First, on hardly reducible (tungsten loadings <15 wt%) or slightly reduced (below 423 K) surfaces, a purely acidic monomolecular mechanism for both isomerization (largely predominant) and cracking reactions, associated with W^{6+} and W^{5+} surface species, was demonstrated. Second, on easily reducible (tungsten loadings >15 wt%) or deeply reduced (over 723 K) surfaces, a bifunctional mechanism associating dehydrogenating/hydrogenating properties occurring on metallic tungsten and acidic isomerization and cracking on W^{5+} and W^{6+} surface species was observed. However, in this last case, we could not exclude the participation of a purely metallic isomerization mechanism occurring through σ-alkyl adsorbed species on the β-W metallic phase. A more pronounced reduction then led to an increase in the extensive hydrogenolysis mechanism, causing catalyst deactivation.

Keywords: Tungsten oxide-supported zirconia; Isomerization; Mechanistic studies; Acidic mechanism; Metallic mechanism; Difunctional mechanism; Correlation with XPS; Surface reducibility

1. Introduction

Catalytic transformations of hydrocarbons, such as alkylation and cracking, are very important in the field of petroleum chemistry. An isomerization process involving the skeletal rearrangement of the starting hydrocarbon molecule to obtain high-octane isoparaffins has been investigated [1–16]. This process, which requires acidic properties, was first investigated using liquid-phase systems such as HF, H_2SO_4 superacids, and halogen-containing solids. Those catalysts exhibited good catalytic performance, but they generated many problems, including corrosion and storage issues. The need for materials in agreement with environmental concerns and regulations has led to the preparation of solid acid catalysts with particular capacities, including (i) high conversion and selectivity toward isomerization, (ii) stability under reaction, (iii) low sensitivity to poisoning, and (iii) easy regeneration. Metal oxide catalysts using oxoanions appear to be suitable candidates for the izomerization of alkanes heavier than C_4. Zirconia modified by sulfate anions, first introduced by Hino and Arata [17], was widely studied because of its high activity and very interesting isomerization selectivity. But sulfate loss during thermal treatment, as well as deactivation of the material during the catalytic reaction, brought Hino and Arata [18] to take an interest in tungsten

* Corresponding author. Fax: +33 3 9 0 24 27 61.
E-mail address: vkeller@chimie.u-strasbg.fr (V. Keller).

0021-9517/$ – see front matter
doi:10.1016/j.jcat.2008.02.026

oxide-supported zirconia. They concluded that superacid sites were created by the interaction of WO_3 with ZrO_2 when the latter oxide was crystallized from an amorphous form into a tetragonal form.

WO_3/ZrO_2 catalysts are usually prepared by wet impregnation of zirconium hydroxide with an appropriate salt solution. It was found that catalytic activity is strongly dependent on both the precursor loading and the calcination temperature, the latter allowing expulsion of the tungstate from the bulk of the aerogel. Maximum catalytic activity was reported to occur for tungsten loadings close to theoretical monolayer coverage of approximately 6.25 W-atoms/nm^2 [19] calculated from the spreading of a single tungsten oxide layer on the support; however, no activity has been reported for catalysts prepared by direct impregnation of crystallized ZrO_2 as obtained when salts were deposited directly on alumina by an equilibrium adsorption technique.

The first part of this report [20] dealt mainly with preparation and characterization methods (in particular, XPS and DRX measurements) of a series of WO_3/ZrO_2 catalysts in which tungsten contents varied from 9 to 30% (-W wt%), obtained by impregnation of a monoclinic zirconium oxide, ZrO_2. Spectroscopic studies revealed that modifications of the catalyst surface occurring during reduction treatments were more or less pronounced and were correlated with tungsten loading. These surface modifications expressed changes in tungsten oxidation state as well as in atomic surface ratio. Consequently, it seems obvious that the catalytic properties of WO_3/ZrO_2 systems strongly depend on the degree of reduction of tungsten surface species. To determine the active sites, it seems necessary to correlate the surface state and the structure obtained by the various surface or volume characterization techniques with the results of catalytic tests. Although the reactivity of alkanes on WO_3/ZrO_2 systems has been extensively investigated, to the best of our knowledge, a direct correlation with the various oxidation states of tungsten determined by X-ray photoelectron spectroscopy (XPS) has not yet been reported.

We also investigated the catalytic behavior of a series of WO_3/ZrO_2 catalysts toward 2-methylpentane and its associated olefin (4-methyl-1-pentene) reactivity. This reactivity was studied as a function of tungsten loading and of the preparation method—direct impregnation of commercial monoclinic ZrO_2, or impregnation of an amorphous hydroxide $ZrO_x(OH)_{4-2x}$ (obtained from the hydrolysis of $ZrOCl_2$)—depending on both the prereduction and reaction temperatures. We also conducted a detailed analysis of cracking and reaction product distribution as a function of reduction duration and carbon chain length, and investigated different reaction mechanisms and their possible correlations with tungsten surface oxidation states.

2. Experimental

2.1. Catalyst preparation

Supported catalysts samples were prepared by wet impregnation with an ammonium metatungstate pentahydrate $(NH_4)_{10}W_{12}O_{41}\cdot 5H_2O$ salt, at pH values close to 5, and deposited either directly on a commercial monoclinic ZrO_2 zirconium oxide (Johnson Matthey) or on an amorphous hydroxide, $ZrO_x(OH)_{4-2x}$, prepared according to the procedure described by Hino and Arata [18]. Whatever the preparation method, impregnation with the ammonium salt was performed in large excess of water, followed by a slow evaporation of the solvent at 373 K and drying overnight at 393 K.

2.1.1. Direct impregnation on commercial monoclinic ZrO_2

The direct impregnation of $(NH_4)_{10}W_{12}O_{41}\cdot 5H_2O$ on a commercial monoclinic ZrO_2 was achieved by calcination of the sample for 1 h in air at 623 K by applying a 5 °K/min ramp. The impregnation of a theoretical monolayer of WO_3 was done supposing that one WO_3 molecule occupied 23 Å^2 [1]. Catalysts with various initial WO_3 contents were prepared by varying the concentration of the precursor salt to obtain initial tungsten weight percentages of 6 (equivalent of one monolayer), 9, 15, 20, and 30%. These catalysts samples were designated WZAm, WZA9, WZA15, WZA20, and WZA30, respectively.

2.1.2. Impregnation on amorphous hydroxide, $ZrO_x(OH)_{4-2x}$

This synthesis proceeded in two successive steps: (i) precipitation of an amorphous phase of zirconium hydroxide, $ZrO_x(OH)_{4-2x}$, obtained from the hydrolysis of $ZrOCl_2$ using the controlled addition of NH_4OH (14,8 N) to maintain a constant pH of 10, with the gel washed and then dried overnight at 293 K, and (ii) wet impregnation of the dried amorphous phase with a solution of $(NH_4)_{10}W_{12}O_{41}\cdot 5H_2O$ precursor. The postsynthesis treatment involved drying the solid overnight at 293 K, followed by calcination for 1 h in air at 1073 K by applying a 10 °K/min ramp. Only one tungsten content sample was prepared in this manner, yielding a 9 wt% W WO_3/ZrO_2 sample designated WZB9.

2.2. Characterization techniques

All of the samples were characterized by XPS, XRD, BET specific surface area, and temperature-programmed reduction (TPR) measurements, as described in detail elsewhere [20].

2.3. Apparatus and procedures

Experiments were performed in a glass flow reactor as described previously [21], equipped with a purification trap to remove oxygen traces. Reactions were carried out under pressure slightly higher than the atmospheric pressure with a 30 cm^3/min flow rate of hydrogen. Five microliters of reactant were injected via a septum into a U-tube maintained at a constant vapor pressure of hydrocarbon (around 6.5 Torr). Reaction products were analyzed by online gas chromatography (Varian 3300) using a dimethylsulfoxane column (50 cm long and 0.3 mm internal diameter) (Chrompack CP-SIL-5CB), with a flame ionization detector and a flux of helium as the gas carrier. Reaction products could be directed through a hydrogenator (Pt Adams) in which molecules were hydrogenated, facilitating chromatographic analysis when working with olefins.

2.4. Probe molecules

The main hydrocarbons used for catalytic tests were 4-methyl-1-pentene (4M1Pen) and 2-methylpentane (2MP). Comparing these two reactants provided information about the acidic and metallic properties of bifunctional catalysts. We also investigated the influence of carbon chain length by studying the reactivity of the linear alkenes 1-hexene (nC_6=), 1-heptene (nC_7=), 1-octene (nC_8=), and 1-nonene (nC_9=).

2.5. Calculations

The total conversion, α_t (%), is defined as the percentage of reactant transformed. The selectivity, S (%), of a product is the percentage of this product among all the products formed. The total reaction rate, r (mol/s g), is defined as the number of moles of reactant transformed per second per gram of catalyst. Starting from 2MP or from 4M1Pen, the 3MP/nC_6 (3-methylpentane/nC_6) ratio can be representative of the acidity of the catalyst, because under acidic reaction conditions, a skeletal rearrangement leads preferentially to the most stable carbocation yielding 3MP.

3. Catalytic results

3.1. Reactivity of 2MP and 4M1Pen

From a thermodynamic standpoint, isomerization reactions are slightly exothermic and are favored at low temperature. The catalysts used for this reaction also must work at the lowest temperature. Based on these considerations, the main reaction temperatures investigated were 473 and 623 K. Different prereduction temperatures also were investigated: 473, 623, 723, and 823 K. It is important to notice that whatever the prereduction duration at 473 and 623 K, WZAm, WZA9, and WZB9 catalysts were not active for 2MP transformation.

Fig. 1a shows the evolution of total conversion (α_t), isomerization (S_{isom}) and cracking (S_{crack}) product selectivities, and 3MP/nC_6 ratio on the WZAm sample when starting from 4M1Pen reacting at 473 K. The catalyst was immediately active for olefin conversion (57%) with high isomerization selectivity (85%). The isomerization ratio value of 3MP/nC_6 was close to 7. These parameters were quite stable with time on stream under hydrogen at 473 K. A slight increase in isomerization selectivity occurred, at the expense of cracking products, to reach stable selectivity of around 93%.

Fig. 1b shows the evolution of the same parameters shown in Fig. 1a (α_t, S_{isom}, S_{crack}, 3MP/nC_6) plus products issued from carbon chain enlargement, $S_{>C_6}$, as a function of prereduction temperature on WZAm sample for 4M1Pen reaction occurring at 473 K. It must be mentioned than the values reported for the reduction temperatures of 473 and 623 K were obtained after reduction of the catalyst for 24 h under hydrogen. In contrast, the values for reduction at 723 and 823 K are associated with 1 h of catalyst prereduction. From Fig. 1b, it can be seen that the olefin reactivity certainly revealed a stable catalyst surface under hydrogen after reduction at 473 and 623 K, but reduction at 723 K modified the catalytic properties of the WZAm system. Indeed, a significant drop in conversion—from 63 to 38%—occurred after reduction at 723 K. This decreased conversion was accompanied by an increase in isomerization selectivity to 100%. A more severe reduction at 823 K led to quasi-inactivity of the system toward conversion of 4M1Pen at 473 K.

Like the WZAm catalyst, the WZA9, WZB9, WZA15, and WZA30 catalysts were immediately active and stable for 4M1Pen isomerization at 473 K without previous reduction and demonstrated high selectivity in isomers (>78%); thus, results of these catalytic tests as a function of reduction duration at 473 K are not given here. In the same manner, results obtained after reduction of the WZA9 catalyst at 623 K (Fig. 2a) are quite similar to those obtained on the WZAm catalyst submitted to the same treatment; however, unlike for the WZAm catalyst, reduction at 723 K did not modify product selectivity to any great degree. A drop in conversion from 58 to 22% was only when reduction temperature was increased from 723 to 823 K. While isomerization selectivity increased (>97%), selectivity

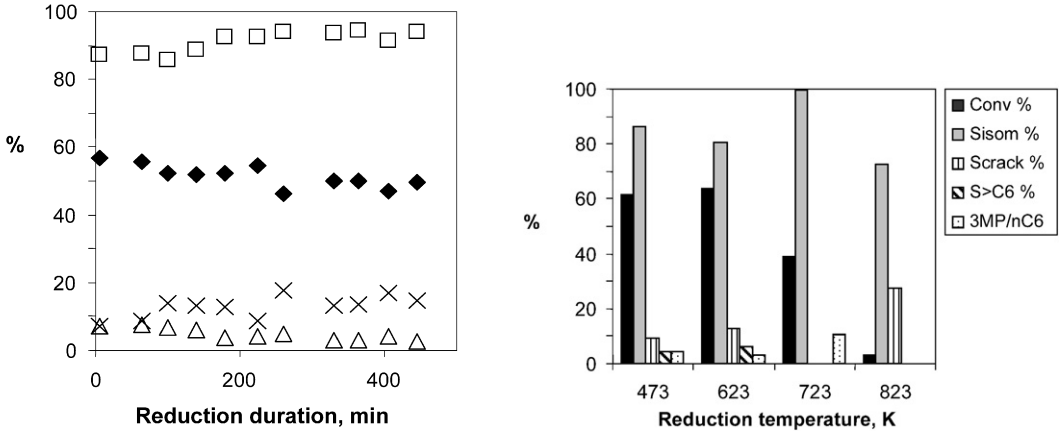

Fig. 1. (a) Evolution of total conversion (%) (◆), of total isomerization (□) and total cracking (△) selectivities (%) and of 3MP/nC_6 (×) ratio as a function of reduction duration (min) at 473 K for 4M1Pen reaction at 473 K on WZAm catalyst. (b) Evolution of total conversion (%), of total isomerization and total cracking selectivities (%), of 3MP/nC_6 ratio and of enlargement reaction products selectivity (%) as a function of reduction temperature for 4M1Pen reaction at 473 K.

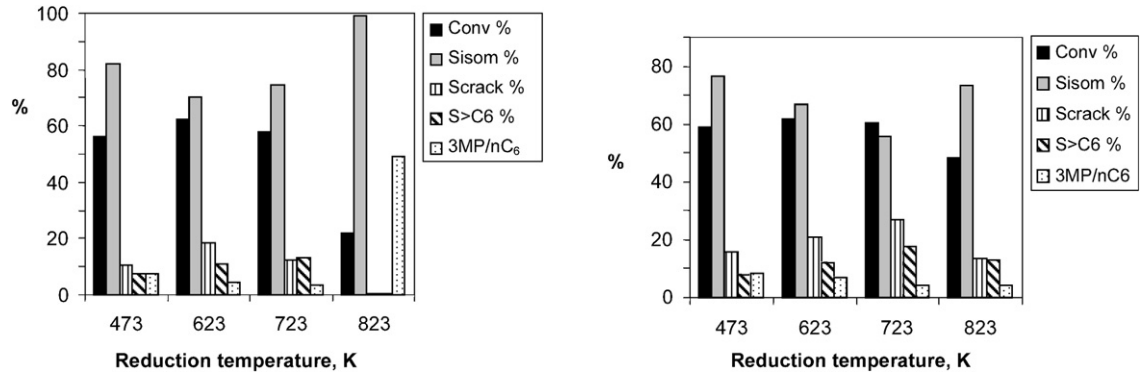

Fig. 2. (a) Evolution of total conversion (%), of total isomerization and total cracking selectivities (%), of 3MP/nC_6 ratio and of enlargement reaction product selectivity (%) as a function of reduction temperature for 4M1Pen reaction at 473 K on WZA9. (b) Evolution of total conversion (%), of total isomerization and total cracking selectivities (%), of and 3MP/nC_6 ratio and of enlargement reaction product selectivity (%) as a function of reduction temperature for 4M1Pen reaction at 473 K on WZB9.

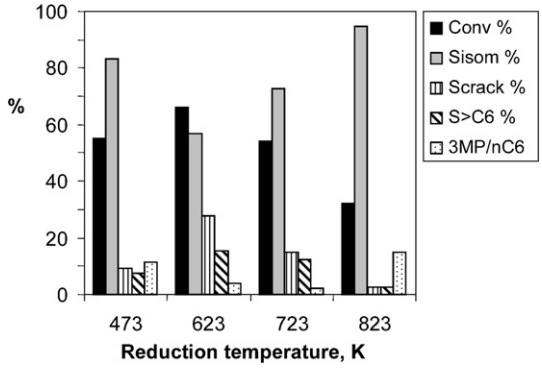

Fig. 3. Evolution of total conversion (%), of total isomerization and total cracking selectivities (%), of 3MP/nC_6 ratio and of enlargement reaction product selectivity (%) as a function of reduction temperature for 4M1Pen reaction at 473 K on WZA15.

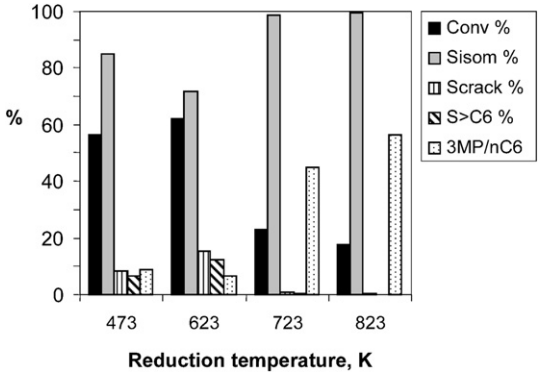

Fig. 4. Evolution of total conversion (%), of total isomerization and total cracking selectivities (%), of 3MP/nC_6 ratio and of enlargement reaction products selectivity (%) as a function of reduction temperature for 4M1Pen reaction at 473 K on WZA20.

in cracking products and products emerging from carbon chain enlargement reactions diminished to quasi-zero values. Fig. 2b shows the conversions and selectivities obtained on WZB9 catalyst as a function of reduction temperature. The isomerization selectivities obtained were lower than those found for the WZA9 catalyst regardless of the reduction temperature. Moreover, the loss of activity after reducing treatments at 823 K was much less pronounced on the catalyst prepared according to the B way.

As for the WZA9 and WZB9 catalysts, a long reduction treatment (24 h) at 473 K (Fig. 3) did not modify the catalytic properties of the WZA15 system for reactions occurring at 473 K. Furthermore, reductions at 623 K (24 h) and at 723 K (1 h) led to the same evolution in properties as for the WZA9 catalyst. A more severe reduction at 823 K (1 h) yielded a decrease in conversion, accompanied by an increase in isomerization of up to 95%. Catalytic tests performed at 623 K when starting from the saturated 2MP molecule revealed activity of the WZA15 catalyst prereduced at 723 K. Conversion of 2MP increased progressively from 12 to 23% in the course of reduction at 723 K, reaching a stable value after 23 h (detailed results not shown). This reactivity of 2MP suggests the presence of catalytic sites that are able to activate the saturated hydrocarbon.

Table 1
Conversion α_T (%), total isomerization S_{isom} and total cracking S_{crack} selectivities (%), 3MP/nC_6 ratio and enlargement reaction products selectivity $S_{>C_6}$ (%) for 4M1Pen reaction at 473 K on WZA20 and WZA30 samples progressively reduced at 723 K

Catalyst	Time (min)	α_T (%)	S_{isom} (%)	S_{crack} (%)	$S_{>C_6}$ (%)	3MP/nC_6
WZA20	60	59.0	66.5	22.0	11.5	1.9
	345 (∼6 h)	32.5	95.0	2.5	2.5	16.4
	1380 (∼24 h)	22.5	98.5	1.0	0.5	44.8
WZA30	60	42.0	91.5	4.5	4.0	6.6
	345 (∼6 h)	44.0	87.0	6.5	6.5	7.3
	1020 (∼17 h)	5.0	98.5	1.5	0	111.3

Fig. 4 illustrates the evolution of conversion and product selectivity of 4M1Pen reacting at 473 K as a function of reduction temperature on the WZA20 catalyst. The figure does not show the evolution of the same parameters observed on the WZA30 sample, because those parameters exhibited similar tendencies in the two catalysts. Both catalysts (WZA20 and WZA30) were active, stable, and selective toward isomerization of 4M1Pen when prereduced at 473 K (24 h) and 623 K (24 h), even with the diminished isomerization selectivity seen at high prereduc-

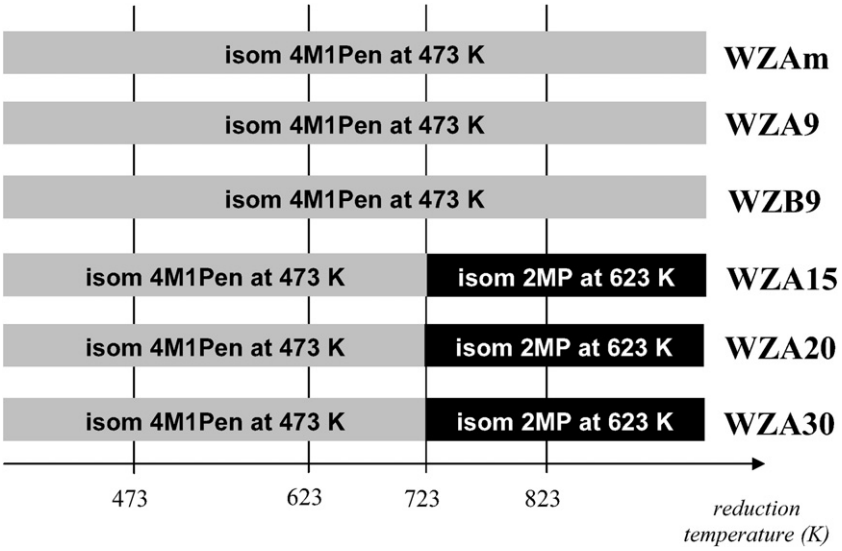

Fig. 5. Evolution of the catalytic properties obtained on WO_3/ZrO_2 samples as a function of tungsten loadings and reducing treatments.

Table 2
Conversion α_T (%), total isomerization S_{isom} and total cracking S_{crack} selectivities (%), 3MP/nC_6 ratio and enlargement reaction products selectivity $S_{>C_6}$ (%) as a function of reduction duration at 723 K for 2MP reaction at 723 K on WZA20 and WZA30 samples

Catalyst	Time (min)	α_T (%)	S_{isom} (%)	S_{crack} (%)	$S_{>C_6}$ (%)	3MP/nC_6
WZA20	345 (∼6 h)	14.0	86.5	13.5	0	4.1
	1380 (∼23 h)	22.0	73.5	26.5	0	8.8
WZA30	205	16.5	87.0	13.0	0	6.9
	1020 (∼17 h)	10.0	42.5	57.5	0	–

tion temperature. Table 1 presents the conversions and product selectivities obtained on the WZA20 and WZA30 systems reduced at 473 K; the table clearly indicates that their activities toward 4M1Pen reacting at 473 K were not stable and decreased over the course of reduction. This decrease was more pronounced on the WZA30 catalyst. Like the WZA15 catalyst, the WZA20 and WZA30 catalysts were active for 2MP isomerization at 623 K when activated at 723 K (Table 2). With increasing duration of reduction at 723 K, the WZA20 catalyst exhibited an increase in 2MP conversion from 14 to 22%, whereas, the WZA30 catalyst showed a decrease in conversion accompanied by a considerable decrease in isomerization selectivity.

Fig. 5 summarizes the evolution of catalytic properties of the different WO_3/ZrO_2 samples as a function of W loading and of reduction treatment. The WO_3/ZrO_2 systems can be classified into two categories of catalysts: (i) those with tungsten loading <15 wt% and (ii) those with tungsten loading >15 wt%. In the first category, the catalysts are active for olefin conversion only at 473 K, whereas the catalysts in the second category exhibit conversion of the saturated 2MP hydrocarbon at 623 K after activation under hydrogen at 723 K.

3.2. Product distributions

Based on the two categories of samples deduced from Fig. 5, herein we discuss only the evolution of product distributions emerging from the two representative WZAm and WZA15 samples in detail. Due to the previously mentioned catalytic behavior, we studied the WZAm catalyst for low-temperature reduction treatments (at 473 and 623 K), and studied the WZA15 catalyst for reduction at temperatures of 723 K and above. We investigated the catalytic properties of the WZAm system by varying the carbon chain length from 1-hexene to 1-nonene. For each molecule, a systematic analysis of the product distribution and the isomerization and cracking activation energies was conducted.

3.2.1. Surfaces slightly reduced or hardly reducible: WO_3/ZrO_2 catalysts with tungsten loadings <15 wt%

3.2.1.1. Conversion of 4M1Pen The distribution of reaction products of 4M1Pen carried out at 473 K on the WZAm sample prereduced at 473 K is shown in Table 3a. Several points can be highlighted:

3MP was the most abundant isomer product obtained. The 3MP/nC_6 ratio was generally >1, indicating that monobranched isomer formation is favored over linear isomer formation. This behavior is characteristic of an acid catalysis. 3MP and nC_6 were not found in the thermodynamic ratio (0.96) at 473 K, suggesting that skeletal rearrangement reactions at the surface were not equilibrated and that desorption was not the rate-limiting step.

The main cracking products were isobutane, iC_4, and isopentane, iC_5.

Molecules with higher molecular weight than the starting molecule were formed in nonnegligible proportions. Among these, methylhexanes, such as 2-methylhexane and 3-methylhexane, were predominant. Among the dimethylpentanes, 23DMP was the most abundant. Molecules with eight carbon atoms were formed at trace levels.

3.2.1.2. Conversion of linear olefins: Influence of chain length Figs. 6a, 6b, and 6c show the results of catalytic tests performed using pulses of 1-hexene ($nC_6=$), 1-heptene ($nC_7=$)

Table 3a
Distribution of reaction products for 4MlPen and $nC_6=$ reactions at 473 K on WZAm catalyst progressively reduced at 473 K

Probe molecule	t (min)	α_T (%)	S_{isom} (%)	S_{crack} (%)	$S_{>C_6}$ (%)	Distribution of reaction products									3MP/nC_6	r (nmol/g/s)
						C_3 (%)	iC_4 (%)	nC_4 (%)	iC_5 (%)	nC_5 (%)	23DMB (%)	3MP (%)	nC_6 (%)	$>C_6$ (%)		
4MlPen	5	57.0	87.0	7.0	6.0	0.3	2.6	0.2	3.7	0.2	14	64.2	8.9	5.7	7.2	1.5
	445	47.0	91.0	4.0	5.0	0.2	1.5	0.2	2.3	0.1	7.1	79.4	4.6	4.6	17.1	1.1
1-Hexen	5	40.0	87.0	7.5	5	0.6	2.8	0.3	3.5	0.3	7.5	41.8	37.7	5	1.1	0.22
	180	24.5	93.5	4.5	2	0.2	1.9	0.1	2.3	0.1	5.7	45.8	41.9	2	1.09	0.12
	390	22.5	95.5	4.5	0	0.1	1.2	0	1.6	0	5.5	46.5	43.2	2.9	1.07	0.11

C_3: propane; iC_4: isobutane, nC_4: *n*-butane, iC_5: isopentane, nC_5: *n*-pentane, 23DMB: 2,3-dimethylbutane.

Table 3b
Distribution of reaction products for $nC_7=$ reaction at 473 K on WZAm catalyst progressively reduced at 473 K

t (min)	α_T (%)	S_{isom} (%)	S_{crack} (%)	Distribution of reaction products (%)													r (nmol/g/s)
				C_2	C_3	C_4	C_5	C_6	22DMP	24DMP	223TMB	33DMP	2MH	23DMP	3MH	3EP	
10	74.0	89.0	11.0	0.3	1.2	3.9	2.8	2.8	1	7.9	0.3	0.1	29.9	12.7	34.5	2.7	0.42
218	71.5	93.0	7.0	0	0.3	2.2	1.9	1.6	1.1	8.1	0.3	0.2	30.2	13.3	37.3	2.8	0.39
1500	57.0	98.5	1.5	0	0.4	0.9	0.1	0	1	7.3	0	0	31.9	12.4	42.5	3.6	0.26

C_2: ethane, C_4: total butanes, C_5: total pentanes, C_6: total hexanes, 22DMP: 2,2-dimethylpentane, 24DMP: 2,4-dimethylpentane, 223TMB: 2,2,3-trimethylbutane, 33DMP: 3,3-dimethylpentane, 2MH: 2-methylhexane, 23DMP: 2,3-dimethylpentane, 3MH: 3-methylhexane, 3EP: 3-ethylpentane.

Table 3c
Distribution of reaction products for $nC_9=$ reaction at 473 K on WZAm catalyst progressively reduced at 473 K

t (min)	α_T (%)	S_{isom} (%)	S_{crack} (%)	Distribution of reaction products (%)										r (nmol/g/s)
				C_3	C_4	C_5	C_6	C_7	C_8	DM*	4MC8	2MC8	3MC8	
16	61.0	93.5	5.5	0.1	2	2	0.7	0.6	1.2	23.2	8.3	36.2	25.8	0.38
190	48.5	98.0	2.0	0	1	1	0	0.3	0	19	6.5	42.8	29.5	0.27
500	33.0	99.0	1.0	0	0.3	0.4	0	0.1	0.1	12.8	7.3	46.1	32.9	0.16

DM*: dimethylpentane isomers, 4MC8: 4-methyloctane, 2MC8: 2-methyloctane, 3MC8: 3-methyloctane.

Table 4
Global, isomerization and cracking apparent activation energies of different hydrocarbons on the WZAm catalyst reduced at 473 K

Starting molecule	Apparent activation energy (kJ/mol)		
	Global	Isomerization	Cracking
4M1Pen	38	35	57
$C_6=$	82	74	144
$C_7=$	91	82	102
$C_8=$	108	108	190
$C_9=$	109	107	219

and 1-nonene ($nC_9=$), respectively, at 473 K. The results obtained with 1-octene are similar to those obtained with $nC_9=$ and thus are not shown here. Table 3 gives the product distributions emerging from $nC_6=$, $nC_7=$, and $nC_9=$. It can be seen that (i) the linear olefins reacted more slowly and had lower conversions than 4M1Pen, (ii) isomers were predominant and increased progressively with reduction time at 473 K, (iii) among the isomers, the monobranched ones were predominant, and (iv) whatever the linear probe molecules tested, the catalyst underwent deactivation, although this did not affect isomerization and cracking selectivity.

3.2.1.3. Kinetic data Apparent activation energies (global, isomerization, and cracking) on the WZAm sample were determined at a temperature range of 423–473 K. Catalytic tests were performed under atmospheric hydrogen pressure and at progressively decreased temperature. Global activation energy was determined by calculating the slope of $\log(r) = f(1/T)$ function. The results for each hydrocarbon are gathered in Table 4. It seems that the apparent activation energy depended on both the branching and the carbon chain length. This activation energy diminished with expanding molecule branching and increased as the carbon chain length went from C_6 to C_8. The lowest activation energy was associated with 4M1Pen (~38 kJ/mol); the highest, with $nC_9=$ (109 kJ/mol). Moreover, it seems that for linear molecules with more than eight carbon atoms, the activation energy was modified only slightly. Whatever the molecule, the isomerization activation energy was lower than the cracking energy. Partial order toward hydrocarbons (not detailed here), deduced from the reaction rate at different hydrocarbon concentrations considering the H_2 carrier gas and reactant as constants, went from 0.76 to 0.97 for $nC_6=$, $nC_7=$, $nC_8=$, and $nC_9=$.

3.2.2. Surfaces deeply reduced or easily reducible: WO_3/ZrO_2 catalysts with tungsten loading ⩾15 wt%

Table 5a shows the evolution of reaction distribution products for the 2 MP and 4M1Pen reactions at 623 K on the WZA15 catalyst as a function of reduction time at 723 K. Important findings include that the olefin reacted more readily than the corresponding alkane, and that methane and ethane (which

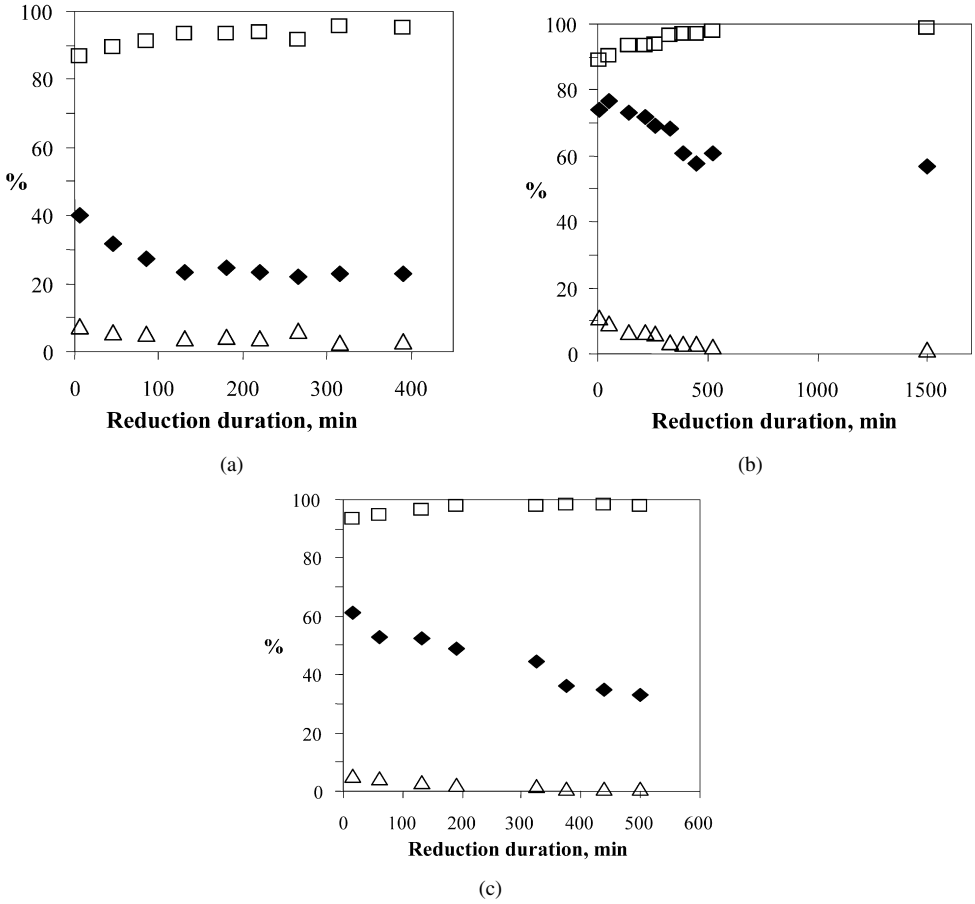

Fig. 6. Evolution of total conversion (◆) (%), of total isomerization (□), and total cracking (△) selectivities (%) as a function of reduction duration (min) at 473 K for (a) 1-hexene ($nC_6=$), (b) 1-heptene ($nC_7=$) and (c) 1-nonene ($nC_9=$) reactions on WZAm catalyst.

Table 5a
Distribution of reaction products for 4MlPen and 2MP reactions at 623 K on WZA15 catalyst progressively reduced at 723 K

Probe molecule	t (min)	α_T (%)	S_{isom} (%)	S_{crack} (%)	$S_{>C_6}$ (%)	Distribution of reaction products (%)										3MP/nC_6	r (nmol/g/s)
						C_1	C_2	C_3	C_4	C_5	22DB	23DB	3MP	nC_6	$>C_6$		
4MlPen	60	62.0	87.5	11.5	1.0	0.5	1	5.3	2.4	2.4	1.8	9.3	35.6	40.6	1.4	0.9	1.7
	480	51.5	89.0	10.5	0.5	1	1.3	2.2	2.1	3.8	2.5	9	55.6	22.1	0.3	2.5	1.9
	1400	52.5	82.0	17.5	0.5	2.2	2.5	3.8	3.7	5.5	2.2	8	52.2	19.7	0.3	2.7	1.2
2MP	60	12.5	90.5	7.5	2	0.8	0.8	2.3	1.3	2.5	2.5	13.1	45.9	28.8	2	1.6	0.16
	480	23.0	71.5	28.5	0	4.5	3.9	5.1	5.4	9.5	1.6	7	55.7	7.2	0	7.7	0.43
	1400	22.0	73.5	26	0.5	4.4	3.8	5.3	4.9	7.6	1.9	8.4	49.4	13.6	0.6	3.6	0.24

Table 5b
Distribution of reaction products for 2MP and 4MlPen reactions at 623 K on WZA15, WZA20 and WZA30 catalysts reduced one hour at 823 K

Probe molecule	Catalyst	α_T (%)	S_{isom} (%)	S_{crack} (%)	Distribution of reaction (%)											3MP/nC_6	r (nmol/g/s)
					C_1	C_2	C_3	iC_4	nC_4	iC_5	nC_5	22DMB	23DMB	3MP	nC_6		
2MP	WZA15	10.0	93.0	7.0	1	0.6	1.4	0.7	0.9	1.5	0.9	1	10.8	73	8.2	9	0.13
	WZA20	35.5	24.0	76.0	5.7	5	6.4	3	3.2	4.6	3.6	2.1	6.8	48.2	11.4	4.2	0.45
	WZA30	6.0	24.0	76.0	12.9	10	16.6	9.1	3.8	13.2	10.5	0	8.9	12.4	2.6	4.8	0.07
4MlPen	WZA20	48.0	81.5	18.5	2.4	2.5	3.7	1.9	1.9	3.7	2.3	2.2	6.8	57.6	15	3.9	0.92
	WZA30	16.5	53.5	46.5	6.4	6.1	10.5	5.3	3.1	9.1	6.2	1.9	1.9	46.7	2.9	16.2	0.29

were not present in the previous experiments with slightly reduced surfaces) were formed when the catalyst was prereduced at 723 K, and their relative proportions increased progressively with reduction time at 723 K.

Table 5b shows the product distribution evolution for the 2MP and 4M1Pen reactions at 623 K as a function of reduction at 823 K on the WZA15, WZA20 and WZA30 catalysts. The table clearly indicates that cracking product proportions

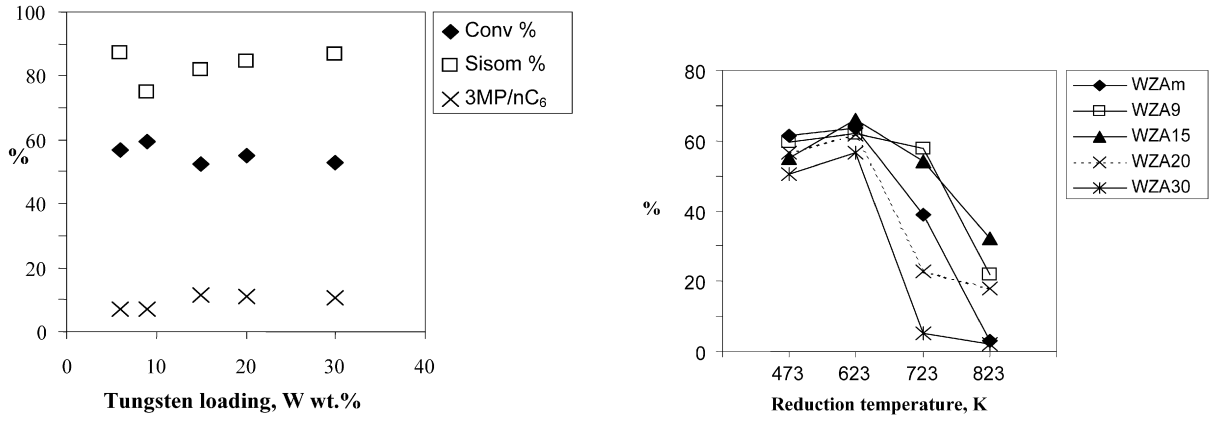

Fig. 7. (a) Initial conversion, total isomerization selectivity(%), and 3MP/nC_6 ratio as a function of tungsten loading for 4M1Pen reaction at 473 K. (b) Evolution of total conversion as a function of reduction temperature for 4M1Pen reaction at 473 K.

increased considerably with tungsten loading when starting from 2MP at the expense of isomerization product selectivity. The activation energies determined on the WZA15 catalyst at 573–623 K were 31 kJ/mol when starting from 4M1Pen and 109 kJ/mol when starting from 2MP (not shown).

4. Discussion

4.1. Influence of the ZrO_2 structure on catalytic activity

As noted in Section 1, few papers deal with the study of WO_3/ZrO_2 catalysts obtained by impregnation of a preformed monoclinic zirconium oxide. WO_3/ZrO_2 is qualified as superacid by Arata and Hino [22] when the catalyst is obtained by impregnation of an amorphous zirconium hydroxide, $Zr(OH)_{4-2x}$. These authors asserted that acid sites are formed by a combination of tungsten oxide with zirconium oxide when the system adopts a tetragonal structure during the calcination step. Several authors have noted that the presence of tungsten oxide species on monoclinic zirconium oxide support does not make the catalyst active for isomerization reactions [23]; the monoclinic WO_3/ZrO_2 system has exhibited only a weak acidity [24]. Although these findings are often cited, they have been experimentally verified only rarely. At the opposite end, the WO_3/ZrO_2 catalysts of our study with a monoclinic zirconium oxide support demonstrated significant isomerization activity both toward olefin (4M1Pen) and saturated molecule (2MP) when reduced sufficiently (for tungsten loading $\geqslant$15 wt%). Moreover, the results obtained for the WZA9 and WZB9 solids demonstrate a similar behavior of both catalysts regardless of the support structure (monoclinic or tetragonal). The absence of activity toward 2MP on the WZA9 and WZB9 catalysts suggest that these systems cannot be considered strong solid acids or superacids, as they have been described according to the Hammet indicators method. But the WZA9 and WZB9 catalysts were immediately active for 4M1Pen conversion. It must be noted that the support structure of the WZA9 remained monoclinic after reducing treatments at 823 K, suggesting no association between isomerization ability and the support's tetragonal structure.

4.2. Influence of tungsten loading on initial catalytic activity

Fig. 7a represents the initial total conversion, isomerization selectivity, and 3MP/nC_6 ratio as functions of tungsten loading for the 4M1Pen reaction at 473 K. It seems that the increase in tungsten species density at the surface of monoclinic ZrO_2 support did not change the initial activity of the WO_3/ZrO_2 samples, or their acidity. Those results are in contradiction with those reported in the literature [25–27] for systems obtained by impregnation of an amorphous zirconium oxide (although in previous studies, the reactant was not 4M1Pen, but heptane, pentane, and xylenes). Hua and Sommer [25], Santiesteban et al. [26], and Barton et al. [27] reported a maximum activity for tungsten loading slightly higher than the monolayer coverage; beyond this value, the activity diminished. This maximum has been explained by increases in the number and the force of acid sites with increasing WO_x species density. The incorporation of a hydrogen atom through polytungstate species structures is linked to the latter's ability to delocalize negative charges. In our case, the XPS studies of calcined and reduced surfaces at 473 K [20] revealed that all of the catalysts were essentially constituted of surface W^{6+} ($\sim$70%) and W^{5+} cations ($\sim$30%). Those proportions were modified only slightly during reduction at 473 K. Our results indicate that the activity was essentially associated with the oxidation state of surface tungsten cations, rather than with tungstate species structure or domain sizes. 4M1Pen reactivity was associated only to Brönsted acid sites with weak to moderate acidity. Hydroxyl groups were associated with W^{5+} cations and, to a lesser extent, to monomeric and polymeric W^{6+} cations tetraedrally coordinated, as described in the part I of this study [20].

Contrary to the conclusions of Barton et al. [27], Iglesia et al. [28], and Kuba et al. [29], we believe that W^{5+} cations are not able to initiate alkane isomerization. Indeed, Barton et al. [27] proposed that carbenium ions are formed by a redox process, leading to formation of organic radicals and W^{5+}

Table 6
Evolution of tungsten oxidation states, determined by XPS (M: metallic state) as a function of reduction temperature

Catalyst	Calcined surface	Reduction temperature (K)			
		473	623	723	823
WZAm	+6, +5	+6, +5	+6, +5	+6, +5	+6, +5
WZ9	+6, +5	+6, +5	+6, +5, +4	+6, +5, +4	+6, +5, +4
WZA15	+6, +5	+6, +5	+6, +5, +4	+6, +5, +4, M	+6, +5, +4, M
WZA20	+6, +5	+6, +5	+6, +5, +4	+6, +5, +4, M	+6, +5, +4, M
WZA30	+6, +5	+6, +5	+6, +5, +4	+6, +5, +4, M	+6, +5, +4, M

cations, whereas Kuba et al. [29] proposed that W^{5+} cations exist through $(H^+)_x[(W^{5+})_x(W^{6+})_{n-x}O_{3n}]^{x-}$ centers of sufficient strength to directly initiate isomerization reactions starting from an alkane.

4.3. Influence of reduction temperature on catalytic activity

As expected based on the XPS studies, the catalytic properties of the WO_3/ZrO_2 systems were modified as a function of reduction temperature. As noted in part I of this report [20], the extent of reduction depends essentially on temperature and tungsten loading. According to reduction intensity, four tungsten oxidation states were evaluated by means of XPS studies, W^{6+}, W^{5+}, W^{4+}, and metallic tungsten. Table 6 summarizes the surface oxidation states of tungsten on each catalyst obtained at different reduction temperatures. The correlation between tungsten oxidation states and 4M1Pen and 2MP reactivity allows us to propose the following:

- Regardless of the tungsten loading, and especially for catalysts with tungsten loadings >9 wt%, reduction at 623 K yielded a slight increase in 4M1Pen conversion at 473 K. As indicated in Table 6, reduction at 623 K led to the formation of W^{4+} cations (except for the catalyst with monolayer coverage). Among the oxidation states of tungsten, the W^{4+} cation has received much attention in the literature, especially regarding its catalytic properties [3,5,30]. Generally considered an intermediate state between the hexavalent W^{6+} cation and metallic tungsten, the W^{4+} cation is known for its hydro/dehydrogenating properties when supported on alumina. These properties result from the presence of bulk WO_2, the slightly deformed rutile structure of which confers metallic properties via π electron delocalization throughout the shortest W–W bonds. Generally, the presence of an oxide support significantly affects the length of those bonds, hindering formation of structures with such properties at the interface of weakly loaded catalysts (under monolayer coverage). In our case, the zero activity toward the saturated molecule suggests that the W^{4+} cations did not exhibit hydro/dehydrogenating properties, and that they were formed not through partial reduction of bulk WO_3, but rather by reduction of an octahedric amorphous phase (as described in part I [20]). We believe that W^{4+} cation formation increased catalytic activity not because of the cations' hydrogenating/dehydrogenating properties, as on bulk WO_3, but because of their acidic cracking properties.
- A significant decrease in 4M1Pen conversion (Fig. 7b) occurred after a long reduction (>1400 min) at 723 and 823 K. This decrease was especially significant in highly tungsten-loaded systems, like WZA20 and WZA30. This decreased conversion can be explained by the transformation of W^{6+} and W^{5+} cations, associated with acid sites, into metallic tungsten, or by tungsten diffusion into zirconium oxide. The decrease in conversion was delayed in systems with intermediate tungsten loadings (9 and 15%), in which important W^{6+} and W^{5+} proportions were preserved. Indeed, whereas the metallic tungsten proportion reached ca 35% on the WZA20 and WZA30 catalysts (after a long reduction treatment at 723 K), XPS revealed a value of only 8% on the WZA15 catalyst [20]. This drop in activity occurred after reduction at 823 K, in accordance with the increase in metallic tungsten proportion [20]. Known for its excellent alkane hydrogenolysis properties, metallic tungsten in α-W led to WZA20 and WZA30 deactivation by coke formation. Consequently, the decreased 4M1Pen conversion is associated with the formation of α-W through the reduction of WO_3 crystallites on highly charged catalysts. Present in larger proportions on the WZA20 and WZA30 catalysts, these large crystallites could be more easily reduced (to α-W) compared with the small crystallites on the WZA15 catalyst, which are more directly in interaction with the support.

The general decrease in conversion on increasing duration of reduction and increasing temperature also can be explained by the continually decreasing W/Zr ratio observed for all of the catalysts [20]. A decreased W/Zr ratio indicates a decrease in the number of accessible active sites either by diffusion or by the coverage of tungsten species by the ZrO_2 support, or, in the presence of tungsten metallic particles, by coalescence. The WZAm and WZA30 catalysts were most strongly affected by these phenomena (Figs. 1b and 7b).

4.4. Isomerization and cracking mechanisms on hardly reducible (tungsten loading <15 wt%) or slightly reduced (below 423 K) surfaces

The absence of metallic properties on slightly reduced or hardly reducible surfaces implies a purely acidic isomerization and cracking mechanism. Even if the formation of products with higher carbon chain length than the starting molecule cannot be neglected (<6%), we believe that the isomerization mechanism was essentially monomolecular under our operating

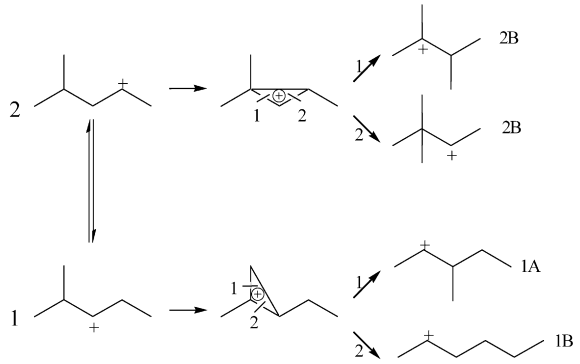

Fig. 8. Methylpentanes and dimethylpentanes formation via protonated cyclopropane.

conditions. Protonation of the linear alkene led only to the formation of a secondary carbocation that did not undergo cracking. Indeed, D-type cracking, leading to the primary cation, was slower than the isomerization of the linear carbocation. The presence of low quantities of linear alkanes among the cracking products is in agreement with those affirmations.

Regarding branched molecules, only a low proportion of propane was observed among the reaction products. This demonstrates that cracking of monobranched alkenes through a C-type mechanism (leading to propane) is not likely. It follows that isomerization of the secondary carbocation is the first step in ion transformation. High isomer product selectivity, regardless of the carbon chain length, suggests that the formation and desorption of the alkene from isomerized carbenium ion is a fast process. Thus, the contact time of carbenium ions at the surface is short, minimizing the likelihood of C–C bond breaking and the consecutive formation of cracking products, especially with increasing carbon chain length of the starting molecule.

Isomerization of 4M1Pen via A- and B-type mechanisms led to 23DMB/22DMB/3MP/nC_6 isomers with a 1/1/1/1 statistical distribution. In our experiments, isomers were formed in the following proportions: 3MP $\gg$ 23DMB $>$ nC_6 $>$ 22DMB. This deviation with respect to statistical distributions can be explained by the thermodynamical stability of the different cationic intermediates. Cyclopropanic intermediates allow us to explain the formation of all isomers without passing through primary carbenium ions, as shown in Fig. 8. The higher selectivity to 3MP compared with dibranched molecules can be explained by a greater stability of the starting carbenium ion, 2-methyl-3-pentylium (1), compared with the 2-methyl-4-pentylium ion (2). The ethyl and isopropyl groups of the former (1) have a greater stabilizing effect than the methyl and isobutyl groups of the latter (2).

A similar hypothesis can be advanced to explain the predominance of 3MP over *n*-hexane and of 2,3-dimethylbutane compared with 2,2-dimethylbutane. This scheme, which implies protonated cyclopropanic intermediates, does not take into account the interaction between molecule and the catalyst surface. Thus we have interpreted the following isomerization mechanism using OH groups that lead to "alkoxy" intermediates, as was first proposed by Cheng and Ponec [31]. When strongly polarized to their ionic form, these alkoxy species can lead to the formation of protonated cycloprotanic intermediates. Fig. 9 illustrates the mechanisms of the different isomers via "alkoxy" species formation by means of a surface Brönsted acid site.

Starting from 1-hexene and considering that isomerization proceeds through B-type isomerization, we can see that the distribution of methylpentanes is close to that expected statistically (cf. Table 3a). Theoretical distribution predicts a 2MP/3MP ratio equivalent to 1, whereas it ranged between 1.07 and 1.1 when catalytic tests were performed at 473 K. This ratio confirms the intervention of a monomolecular mechanism. An analogous scheme to that for 4M1Pen isomerization can explain the formation of methylpentanes. 2-Methyl-3-pentylium and 3-methyl-2-pentylium are formed via the cyclization of *n*-hexyl cation. The formation of 23DMB and 22DMB, starting from 1-hexene, proceeds through consecutive 2-methyl-4-pentylium and 3-methyl-2-pentylium ion isomerization within the same adsorbed phase.

1-Heptene is the first molecule for which no products with a mass exceeding that of the starting molecule have been detected. Weitkamp et al. [32] studied the isomerization of *n*-heptane over zeolithes, distinguishing between monomolecular and bimolecular mechanisms based on the absence or presence of peculiar reaction products. They proposed that 22DMP, 33DMP, and 3EP formation are suppressed on catalysts with bimolecular isomerization properties. All of those hydrocarbons were present in our reaction products, in agreement with the hypothesis of a monomolecular mechanism for 1-heptene. B-type isomerization led to a 1/2 ratio of 2MH and 3MH. Experimentally, this ratio ranged between 0.86 and 0.75, not far from the thermodynamic equilibrium value of 0.82. Deviation to statistical predictions can be explained by the consecutive transformation of the products resulting from the first isomerization step (B-type isomerization) via A-type isomerization until thermodynamic equilibrium is reached.

As reported by Zhang et al. [9], dibranched molecules with one of the two ramifications set on the second carbon are predominant. Weitkamp et al. [33] explained this finding by a decrease in B-type isomerization. The decreased proportion of dimethylpentanes with reaction time was not seen for 3EP, the proportion of which increased among the isomer products with decreasing temperature. According to Weitkamp et al. [32], this finding is in agreement with an isomerization mechanism, and also implies the presence of cyclopropanic intermediates and protonated cyclobutanic intermediates, as was proposed by Martens and Jacobs [34].

At first sight, the increase in global activation energy with carbon chain length (Table 4) may appear surprising if a classical acidic isomerization mechanism is assumed. The adsorption of hydrocarbon generally increases with increasing carbon chain length. This increasing adsorption is in accordance with the increase in cracking products typically observed during acid catalysis with increasing carbon chain length. But, in contradiction to these usual findings, it appears that the products emerging from isomerization reactions were formed preferentially (>95%) even when starting from 1-nonene. This finding is in agreement with a single mode of adsorption (via a double

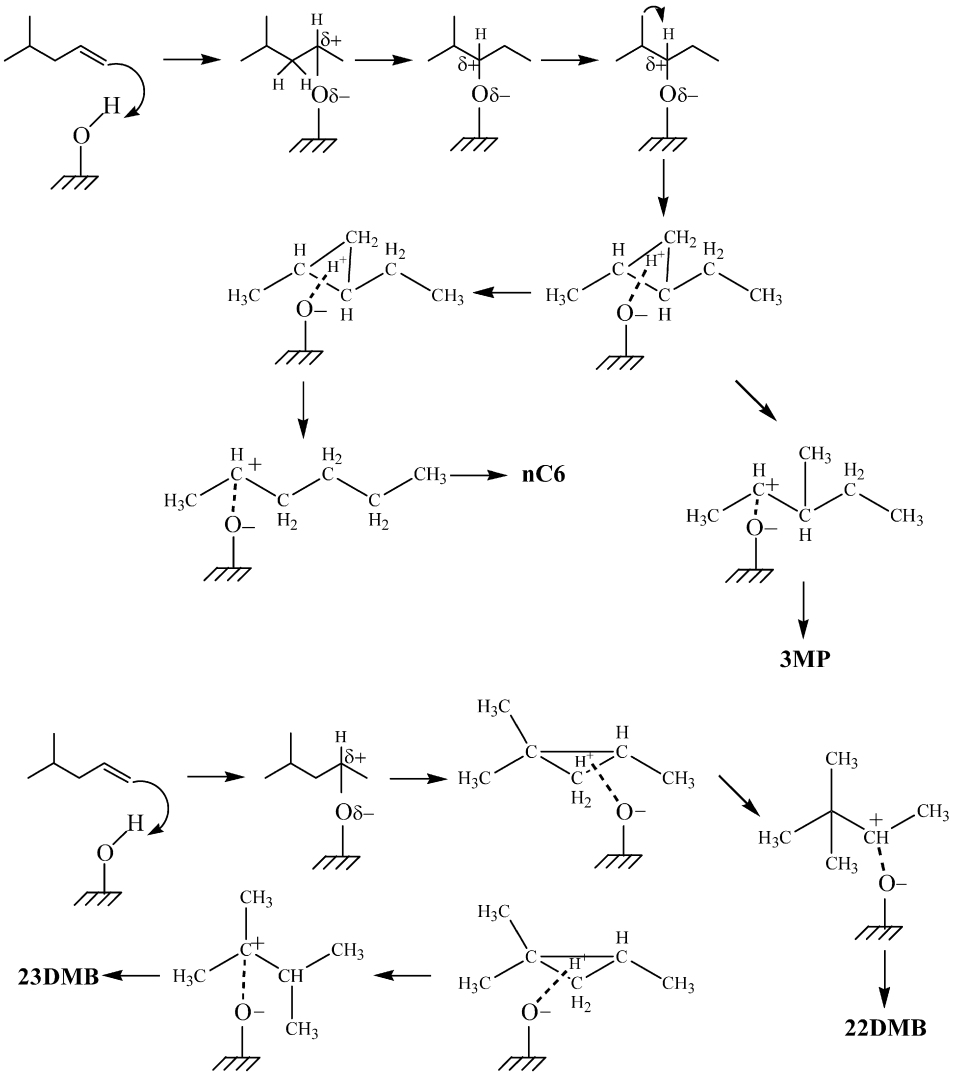

Fig. 9. 4M1Pen isomerization through alkoxy species.

bond in position 1) and reaction of the molecules at the catalyst surface whatever the molecule size. The increase in activation energy from C_6 to C_9 can be explained by a steric effect due to alkyl groups in the β-position with respect to the carbon with the double bond. This steric difficulty increases with the size of the alkyl group, leading to a decrease in the adsorption heat value (ΔH_{ads}), as well as a consecutive increase in activation energy with increasing carbon number of the starting molecule—that is, $E_a = E^0 + \Delta H_{ads}$, with E_a apparent activation energy, E^0, absolute energy, and $\Delta H_{ads} < 0$.

4.5. Cracking mechanisms

When starting from 4M1Pen or 1-hexene, the cracking products ranged from C_3 to C_5. In parallel, products with molecular mass higher than the starting molecule were detected. The absence of methane and ethane starting from 1-hexene indicates that hydrogenolysis and β-scission (not favored energetically due to the formation of primary ions) did not occur. Consequently, we believe, like Santiesteban et al. [35], that formation of the main cracking products (i.e., isobutane and isopentane) resulted from the β-scission of carbenium ion intermediates of high molecular mass formed by enlargement of surface hexyl cations. This supposition is in accordance with the presence of C_7 among the reaction products. Indeed, β-scission of carbenium ions favors the formation of fragments leading to branched alkanes, iC_4 or iC_5, but not the formation of primary carbenium ions leading to C_1 or C_2. Unlike the isomerization mechanism, which implies intramolecular (monomolecular) transformations, cracking of C_6 molecules must proceed through intermolecular (bimolecular) transformations. Analogous conclusions can be drawn for the analysis of cracking products emerging from 1-heptene to 1-nonene.

4.6. Isomerization and cracking mechanisms on easily reducible (tungsten loading >15 wt%) or deeply reduced (over 723 K) surfaces

Comparing the reactivity of 4M1Pen and 2MP at 623 K indicates that on WO_3/ZrO_2 surfaces prereduced at 723 K, the

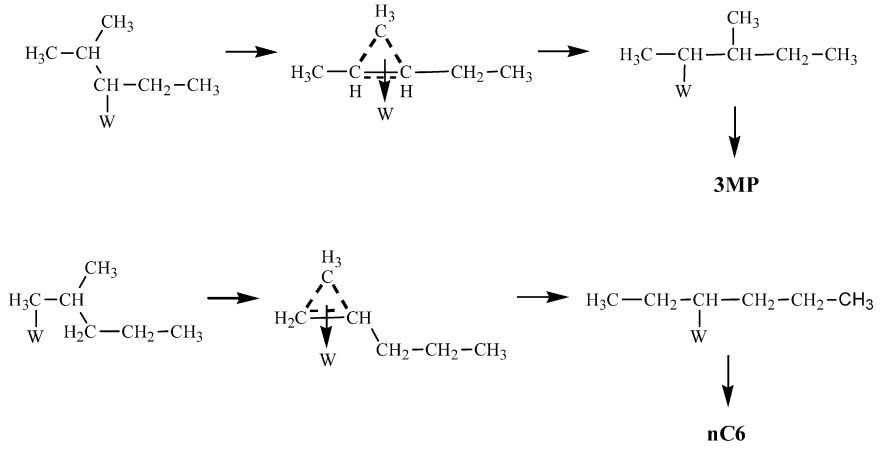

Fig. 10. Isomerization of 2MP via σ-alkyl adsorbed intermediates.

olefin reacted faster than the corresponding alkane (cf. Tables 5a and 5b). This finding suggests that the rate-determining step was the alkane C–H bond rupture. As shown previously, 2MP activation occurs with metallic tungsten formation. So is the isomerization mechanism purely metallic or bifunctional (dehydrogenation/hydrogenation on metallic sites and cracking/isomerization on acidic sites), or do both mechanisms occur? Several findings argue in favor of a bifunctional mechanism in which carbenium ions are implied: (i) the global activation energy value, E_a, obtained for 2MP (109 kJ/mol) is characteristic of a bifunctional catalysis; (ii) the isomerization ratio, 3MP/nC_6, was nearly the same for 4M1Pen and 2MP; and (iii) the proportion of 2DMB was always lower than that of 23DMB, in agreement with the thermodynamic stability of carbenium ions.

In the same manner, several findings suggest a metallic monofunctional mechanism intervention. Among these are the increased proportions of methane and ethane with increasing duration of reduction at 723 K (Table 5). Indeed, the weak possibility of D-type β-scission on acidic sites leading to C_2 suggests formation of demethylation and deethylation products on metallic sites. Another important finding in this regard is the progressive decrease in iC_4/nC_4 and iC_5/nC_5 with increasing intensity of reduction treatment. On acidic cracking (β-scission), hydrogenolysis does not favor the formation of branched molecules.

Apparently, both the bifunctional and the metallic monofunctional mechanisms must be taken into account simultaneously on surfaces reduced at 723 K. Even if determining the relative proportion of each mechanism is difficult, it seems reasonable to suggest that the formation of cracking products is associated with both mechanisms. But the progressive increase in the proportions of C_1 and C_2 with decreasing temperature and tungsten loading (especially for the WZA20 and WZA30 catalysts) indicates an evolution toward a purely metallic mechanism. Both the activation of 2MP and the increase in hydrogenolysis products clearly indicate the existence of two kind of metallic sites on the catalysts reduced at 723 K. This can be explained by, as observed in previous studies on WO_3-based materials [36–38], the progressive transformation during reduction of metallic tungsten initially present in a metastable β-W phase into a α-W phase. Unlike the W_3O phase (β-W), the pure α-W phase obtained by reduction of the W_3O phase essentially has the metallic properties of hydrogenolysis. Note that tungsten metal phases β-W and α-W can coexist and have dehydrogenating and hydrogenating properties.

Previous studies [38,39] have demonstrated that reduction of bulk WO_3 leads to bifunctional catalysts on which the dehydrogenation/hydrogenation function is provided by metallic tungsten. Transformation of the alkene (emerging from alkane dehydrogenation) then follows the aforementioned mechanism with protonated cyclopropanic intermediates on acidic sites.

As was previously observed on partially oxidized tungsten carbides, we associate a nonpredominant metallic-type isomerization to adsorbed σ-alkyl intermediates, like those proposed by McKervey et al. [40]. This occurs on a β-W metallic phase. The σ-alkyl species most energetically favored for isomerization reactions over metallacyclobutane intermediates imply transition species with two electrons and three centers, like those shown in Fig. 10.

Regardless of the duration of reduction, the amounts of methane and ethane obtained were always greater than predicted by the statistical rupture of a single C–C bond ($C_5 + C_1$ or $C_4 + C_2$). This finding clearly suggests consecutive rupture of carbon–carbon bonds of the molecule before its desorption, due to multiple adsorption on the metal. That scheme was first proposed for noble metal particles [41]. Adaptation of this model to our catalysts suggests the presence of metallic tungsten capable of adsorbing the reactant to a significant degree. We assign those metallic sites to a α-W phase, formed by the ultimate reduction of WO_3 crystallites. It is important to note that demethylation and deethylation products were quasi-unformed on the WZA15 catalyst, in which the proportion of metallic tungsten was <9% even after the reduction treatment at 823 K. We believe that for the 15% tungsten-loaded catalyst, the WO_3 crystallites formed during the calcination step were not large enough to be transformed into an α-W phase during reduction treatments. Rather, their reduction led to a β-W phase that was stabilized due to metal–support interactions. These metal–support interactions were less predominant on the

largest WO_3 crystallites, such as those formed on the WZA20 and WZA30 catalysts. This phenomenon makes the WZA15 catalyst a stable system for hydrocarbon isomerization.

5. Conclusion

WO_3/ZrO_2 catalysts with different tungsten loadings were evaluated for isomerization of hydrocarbons. In contradiction to previous studies, here we found that the crystallographic structure of the zirconium oxide had no influence on catalytic properties of WO_3/ZrO_2 systems. Correlations with XPS and XRD measurements [20] allow us to point out two catalytic behaviors:

(i) Hardly reducible (tungsten loading <15 wt%) or slightly reduced (below 423 K) surfaces were immediately active for 4M1Pen conversion but inactive for the saturated molecule transformation. These surfaces were essentially associated with high oxidation surface states of tungsten and especially to W^{6+} and W^{5+}. The weak to moderate acidity, associated mainly with Brönsted acidity, led to a monomolecular mechanism and high isomerization selectivity at 473 K regardless of the carbon chain length. The isomerization selectivity is explained by the formation of "alkoxy" species leading to protonated cyclopropanic intermediates. Cracking reactions (not predominant) proceeded on the most strongly acidic sites.

(ii) Readily reducible (tungsten loading >15 wt%) or deeply reduced (over 723 K) surfaces were active for 2MP transformation at 623 K. This activity is associated with the formation of metallic tungsten through reduction of WO_3 crystallites. Indeed, metallic tungsten has dehydrogenating/hydrogenating properties and confers a mainly bifunctional behavior to the WO_3/ZrO_2 catalyst. Nonetheless, the possibility of a minor effect of a purely metallic isomerization mechanism implying both β-W metallic and more reduced α-W phases cannot be excluded.

After the reduction treatment and tungsten loading, the catalytic properties of WO_3/ZrO_2 were seen to evolve from a purely monofunctional acidic catalysis to a purely metallic one, passing through a bifunctional catalysis. A tungsten loading of 15% seems to be the critical value to ensure high activity, selectivity, and stability of the catalyst on stream and good activity for saturated hydrocarbon isomerization.

References

[1] S. Meijers, L.H. Gielgens, V. Ponec, J. Catal. 156 (1995) 147.
[2] V. Adeeva, G.D. Lei, W.M.H. Sachtler, Appl. Catal. A 118 (1994) L11.
[3] A. Katrib, F. Hemming, P. Wehrer, L. Hilaire, G. Maire, J. Electron. Spectrosc. Relat. Phenom. 76 (1995) 195.
[4] E. Blomsma, J.A. Martens, P.A. Jacobs, J. Catal. 159 (1996) 323.
[5] A. Katrib, V. Logie, N. Saurel, P. Wehrer, L. Hilaire, G. Maire, Surface Sci. 377 (1997) 754.
[6] A. Chica, A. Corma, J. Catal. 187 (1999) 167.
[7] M. Höchtl, A. Jentys, H. Vinek, Microporous Mesoporous Mater. 31 (1999) 271.
[8] A. Lugstein, A. Jentys, H. Vinek, Appl. Catal. A 176 (1999) 119.
[9] W. Zhang, P.G. Smirniotis, J. Catal. 182 (1999) 400.
[10] S. Siffert, J.L. Schmitt, J. Sommer, F. Garin, J. Catal. 184 (1999) 19.
[11] J.F. Denayer, G.V. Baron, G. Vanbutsele, P.A. Jacobs, J.A. Martens, J. Catal. 190 (2000) 469.
[12] V. Keller, F. Barath, G. Maire, J. Catal. 189 (2000) 269.
[13] V. Calemma, S. Peratello, C. Perego, Appl. Catal. A 190 (2000) 207.
[14] W. Hua, A. Goeppert, J. Sommer, J. Catal. 197 (2001) 406.
[15] A. Katrib, D. Mey, G. Maire, Catal. Today 65 (2001) 179.
[16] Y. Rezgui, M. Guemini, A. Tiguezza, A. Bouchemma, Catal. Lett. 87 (2003) 11.
[17] M. Hino, S. Kobayashi, K. Arata, J. Am. Chem. Soc. 101 (1979) 6439.
[18] K. Arata, M. Hino, J. Chem. Soc. Chem. Commun. (1987) 1529.
[19] R.A. Boyse, E.I. Ko, J. Catal. 171 (1997) 191.
[20] F. Di Gregorio, V. Keller, F. Garin, J. Catal. 225 (2004) 44.
[21] F. Di Gregorio, V. Keller, T. Di Constanzo, J.L. Vignes, D. Michel, G. Maire, Appl. Catal. A 218 (2001) 13.
[22] K. Arata, M. Hino, in: M.J. Phillips, M. Ternan (Eds.), Proc. 9th Int. Congr. on Catalysis, Calgary Alberta, 1988, The Chemical Institute of Canada, Ottawa, 1988, p. 1727.
[23] Y. Huang, B. Zhao, Y. Xie, Appl. Catal. A 172 (1998) 327.
[24] J.C. Yori, J.M. Parera, Catal. Lett. 65 (2000) 205.
[25] W. Hua, J. Sommer, Appl. Catal. A 232 (2002) 129.
[26] J.G. Santiesteban, J.C. Vartulli, R.D. Bastian, D. Chang, J. Catal. 168 (1997) 431.
[27] D.G. Barton, S.L. Soled, G.D. Meitzner, G.A. Fuentes, E. Iglesia, J. Catal. 181 (1999) 57.
[28] E. Iglesia, D.G. Barton, S.L. Soled, S. Miseo, J. Baumgartner, W.E. Gates, G.A. Fuentes, G.D. Meitzner, in: J.W. Hightower (Ed.), 11th Int. Congr. Catalysis, Baltimore, 1996, Elsevier, Amsterdam, 1996, p. 553, Stud. Surf. Sci. Catal. 101 (1996) 553.
[29] S. Kuba, P. Lukinskas, R.K. Grasselli, B.C. Gates, H. Knözinger, J. Catal. 216 (2003) 353.
[30] W. Grunert, E.S. Shpiro, R. Feldhaus, K. Anders, G.V. Antoshin, K.M. Minachev, J. Catal. 107 (1987) 522.
[31] Z.X. Cheng, V. Ponec, Catal. Lett. 25 (1994) 337.
[32] J. Weitkamp, P.A. Jacobs, J.A. Martens, Appl. Catal. A 8 (1983) 123.
[33] J. Weitkamp, Ind. Eng. Chem. Prod. Res. Dev. 21 (1982) 550.
[34] J.A. Martens, P.A. Jacobs, in: J.B. Moffat (Ed.), Theorical Aspects of Heterogeneous Catalysis, Catalysis Series, Van Nostrand–Reinhold, New York, 1990, Chap. 2.
[35] J.G. Santiesteban, D.C. Calabro, C.D. Chang, J.C. Vartulli, T.J. Fiebig, R.D. Bastion, J. Catal. 202 (2001) 25.
[36] M. Molière, Ph.D. thesis, University of Strasbourg, 1978.
[37] F. Hemming, Ph.D. thesis, University of Strasbourg, 1995.
[38] V. Keller, Ph.D. thesis, University of Strasbourg, 1993.
[39] G. Hägg, N. Schonberg, Acta Crystallogr. 7 (1954) 351.
[40] M.A. McKervey, J.J. Rooney, N.G. Samman, J. Catal. 30 (1973) 330.
[41] F.G. Gault, Adv. Catal. 30 (1981) 1.